(Received 11 January 2024, Accepted 5 April 2024, Scheduled 12 April 2024)

Design of a Simple Four-Port UWB-MIMO Antenna Based on a Fan-Shaped Isolator

Wanying Ren[1], Zhong-Gen Wang[1,*], Ming Yang[2], Jinzhi Zhou[3], and Wen-Yan Nie[4]

[1]*School of Electrical and Information Engineering, Anhui University of Science and Technology, Huainan 232001, China*
[2]*School of Electrical and Communications Engineering, West Anhui University, Luan 237012, China*
[3]*School Electrical and Information Engineering, Bozhou University, Bozhou 236800, China*
[4]*School of Mechanical and Electrical Engineering, Huainan Normal University, Huainan 232001, China*

ABSTRACT: In this paper, a novel, highly isolated ultra-wideband multiple-input, multiple-output antenna design for indoor communication is proposed. The overall size of the antenna is only $36 \times 36\,\text{mm}^2$, and it contains four monopole antenna units and a fan-shaped isolated structure. Each antenna cell is composed of a U-shaped patch element and a defected rectangular ground structure. The fan-shaped decoupling structure effectively absorbs coupling currents, significantly improving isolation. As a result, the proposed antenna system can cover the entire ultra-wideband and receive a resonant frequency of 2–11.08 GHz. The results demonstrate that the antenna's isolation is greater than 15 dB in the operating band. Furthermore, the antenna exhibits good radiation characteristics and reasonable envelope correlation coefficients.

1. INTRODUCTION

Ultra-wideband multiple-input, multiple-output (UWB-MIMO) antenna can transmit a large amount of data within a short distance and is characterized by strong anti-interference ability and fast transmission speed. This antenna can be applied to wireless data transmission, radar detection, indoor positioning, and medical monitoring to improve communication quality and performance. On the other hand, MIMO technology plays a crucial role in improving the data transmission rate and reliability of wireless communication systems. It achieves this by allowing simultaneous transmission of multiple data streams through the use of multiple antennas for transmission and reception. This results in improved spectrum utilization and transmission capacity. Consequently, MIMO technology is considered a key technology in antenna design. By eliminating multipath interference and suppressing noise, it enhances signal quality and system performance [1]. As a result, it is employed in satellite communication systems, mobile communications, WLAN networks, and broadband wireless networks. In 2002, the United States Federal Communications Commission (FCC) officially allocated a frequency band for the deployment of UWB technology. This spectrum, designated for low-power output applications, extends from 3.1 to 10.6 gigahertz [2]. The combination of UWB and MIMO enables higher data speeds and more dependability in wireless communication systems, allowing for increased transmission range without an increase in the antenna's radiated power [3–12].

Several approaches to achieving UWB features include the use of gradual geometry structures [13], resonant structures [14], and slot structures [15–17]. In [13], a small, stepped transmission line (TL)-loaded wideband antenna was introduced and printed on an RT/Duroid 5880 substrate. Its dimensions were $50\,\text{mm} \times 50\,\text{mm} \times 1.52\,\text{mm}$, and it could cover 2.1–11.5 GHz. In [14], a slot and a quarter-wavelength resonator were used to create a wideband antenna with double rejection zeros. By employing this technique, the antenna's bandwidth is increased by up to 32% between 4.2 and 5.6 GHz, and the effectiveness of a filter theory-based feeding network is confirmed. The antenna proposed by Zhang et al. consisted of two antenna elements sharing a radiator to achieve a very small $26\,\text{mm} \times 26\,\text{mm}$ dimension. By installing a rectangular patch on the rear of the radiator and carving an I-beam slot in it, an operating band covering 3.1–10.6 GHz was finally obtained [16].

However, in minimal MIMO antenna devices, the antenna elements will be severely coupled because of the near-field radiation and current flow, which will reduce the antenna's performance. Numerous techniques for decoupling have been suggested, including electromagnetic band gap (EBG), neutralization line (NL), decoupling networks, defective ground structure (DGS), and other techniques to enhance isolation and be compatible with modern portable compact communication devices. In [18], a small, conical MIMO antenna with dual-band notched characteristics was built, and an L-shaped pattern was used to achieve high ground plane isolation below -22 dB. To reduce coupling, Tang et al. proposed a separate staircase-shaped construction [19]. A four-element UWB-MIMO antenna was designed to perform well in terms of compactness and isolation. For UWB wireless communication applications, Iqbal et al. developed an extremely isolated two-element triangular MIMO antenna that had a two-step cutoff at its bottom edge. To im-

* Corresponding author: Zhong-Gen Wang (zgwang@ahu.edu.cn).

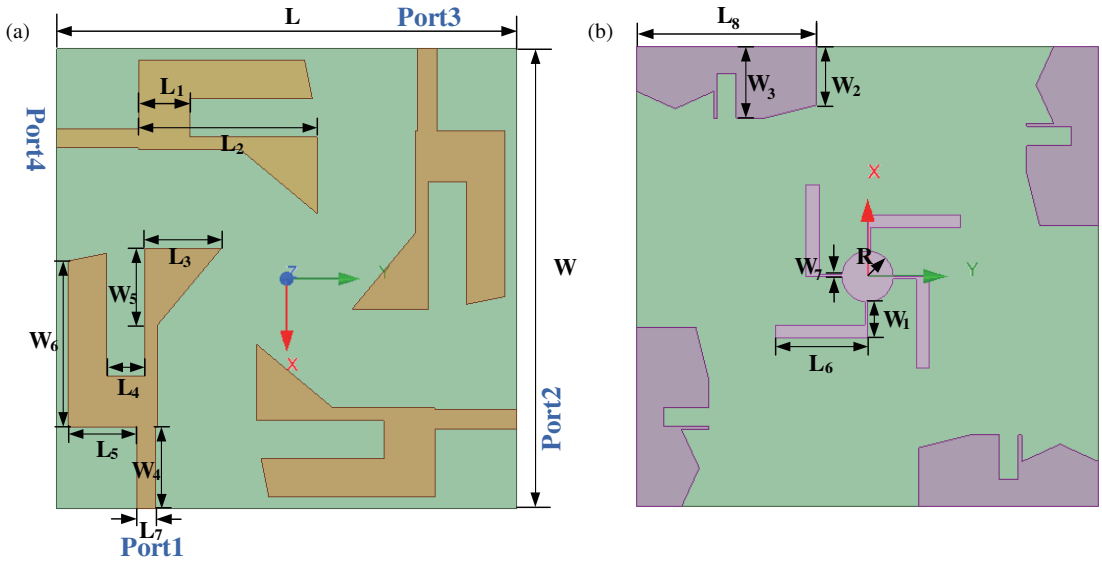

FIGURE 1. Geometrical structure of the proposed four-port MIMO antenna (a) Front structure and (b) Backside structure.

prove the isolation between the radiators, two F-shaped stubs were also added to the ground plane [20]. Similarly, Wang et al. considered a compact, two-element, half-sliced UWB-MIMO antenna. The fence construction consisted of 16 slits that acted as band-stop filters to achieve a high degree of isolation between the radiating elements [21]. The antenna proposed by Lu et al. in [22] consisted of four identical modified elliptical radiators placed orthogonally, and an isolation of better than 18 dB was achieved by etching two inverted L-shaped slots on the radiating elements and by using herringbone line decouplers. The antenna proposed in [23] consisted of four rectangular radiating elements arranged symmetrically and orthogonally on a defective ground plane, with four thin truncations carefully placed in the ground plane's center to form a rectangle with provided corners used to mitigate the mutual coupling between adjacent antenna elements, ultimately obtaining an isolation of more than 18.6 dB. According to [24], adopting open-loop ring resonators permitted greater isolation beyond -15 dB and coverage across a wider band of frequencies, while also reducing the size of the antenna element. A pentagonal radiator combined two symmetrical coordinators. Excellent isolation was achieved by a stub on the ground plane and a radiator T-shaped slot [25]. Due to its size of 93 mm $\times$ 47 mm $\times$ 1.6 mm, the 2×2 UWB-MIMO antenna was not portable but used a decoupling form to attain an isolation greater than 31 dB [26]. In 2×2 MIMO, the stepped arrangement of each radiating element enhanced isolation. Good isolation ($S_{21} < -18$ dB) was further enhanced using a defective ground compact electromagnetic bandgap (DG-CEBG) [27]. High isolation and an extensive bandwidth between 1.99 GHz and 10.02 GHz were accomplished using two identical semi-circular radiating components with an I-shaped ground structure and a symmetrical stepped elliptical structure [28]. The rectangular 4×4 radiators were arranged orthogonally to one another, and each element had a square slit to generate a high isolation of more than 32 dB [29]. The UWB MIMO antenna proposed by Mathur and Dwari consisted of four half-hexagonal monopole antenna elements and provided polarization diversity and reasonable isolation. All antenna elements were placed orthogonally to each other, achieving better than 15 dB isolation between the elements [30]. The flower-shaped UWB-MIMO antenna described in [31] was made up of four symmetrical, flower-shaped radiating components arranged orthogonally to one another to create a composition that produced isolation in the MIMO elements of greater than 18 dB.

In summary, the results of this research demonstrate a novel four-port UWB MIMO antenna structure that contains four fan-shaped radiating elements and a fan-shaped isolation structure. By using orthogonally placed antenna elements and a slotted grounding layer, a more isolated and compact antenna is designed to receive resonant frequencies from 2–11.08 GHz, covering the entire UWB. This 4-port antenna is suitable for indoor communications. The fan-shaped isolation structure ensures effective frequency band isolation of greater than 15 dB. Furthermore, the MIMO antenna exhibits excellent radiation and diversity performance.

2. ANTENNA DESIGN

2.1. Antenna Model

The geometry of the antenna is shown in Fig. 1. The antenna is printed on an FR4 dielectric substrate with total dimensions of 36 mm $\times$ 36 mm $\times$ 0.8 mm, a relative permittivity of 4.4, and a loss tangent of 0.02. Each antenna unit consists of a U-shaped radiating patch and a rectangular metal ground printed on the backplane. The U-shaped radiating patch is printed on the top layer of the substrate, while the rectangular ground is carefully cut to ensure uniformity across all antenna units. Moreover, the antenna units are positioned in pairs and placed orthogonally to enhance inter-element isolation and compactness. Additionally, a small fan-shaped metal isolation structure is strategically placed in the central area of the base plate to efficiently mini-

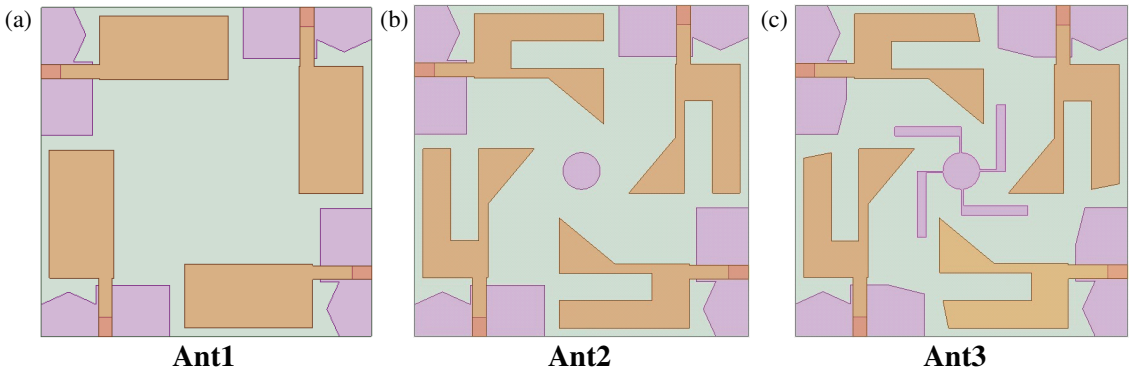

FIGURE 2. The design development of the antenna structure. (a) Ant 1, (b) Ant 2, and (c) Ant 3.

TABLE 1. Optimized parametric dimensions of proposed MIMO antenna.

Parameters	L	L_1	L_2	L_3	L_4	L_5	L_6	L_7	L_8
Value (mm)	36	4	14	5	3	5.35	7	1.5	14
Parameters	W	W_1	W_2	W_3	W_4	W_5	W_6	W_7	R
Value (mm)	36	2.8	5.6	4.6	6.4	6	13	0.2	2

mize coupling between antennas. Table 1 shows the optimized parametric dimensions of the proposed MIMO antenna.

2.2. Antenna Structure Design Analysis

2.2.1. Antenna Structure Design

The corresponding development of the antenna structure is shown in Fig. 2. In Fig. 2(a), four identical antennas with two orthogonal rectangular radiating patches are printed on the substrate's front side, and a regularly cut rectangular ground plane corresponding to each radiating patch is printed on the substrate's back side, which constitutes the basic structure of the antenna, where the frequency of the rectangular patches can be found using the formula below [32]:

$$f = \frac{c}{4L\sqrt{\varepsilon_\gamma}} \tag{1}$$

where ε_γ is the dielectric constant of the FR4, f the resonant frequency, L the effective length of the rectangular patch, and c the electromagnetic wave propagation speed.

As Fig. 2(b) shows, since the basic radiating element does not display enhanced broadband characteristics, it appears that altering the antenna patch's structure is required to obtain these features. To achieve wider bandwidth characteristics and enhance the antenna's impedance matching quality, the distribution parameters of the transmission line are changed by digging out a rectangle on the radiating patch and adding a tiny triangle on the side of the radiating patch. In addition, circular branches are added to the substrate's bottom to provide more coupling routes and enhance the antenna's isolation. The radius of the circular patch (R) may be calculated using the formula given in [33].

$$F = \frac{8.791 \times 10^9}{f_s\sqrt{\varepsilon_\gamma}} \tag{2}$$

$$R = \frac{F}{\left\{1 + \frac{2h}{\pi F \varepsilon_\gamma}\left[\ln\left(\frac{\pi F}{2\pi}\right) + 1.7726\right]\right\}^{\frac{1}{2}}} \tag{3}$$

where h is the thickness of the dielectric substrate, ε_γ the relative permittivity, and f_s the intended resonant frequency.

As depicted in Fig. 2(c), to widen the bandwidth and further increase the isolation, the radiating patch and backplane rectangle are clipped, and the circular isolation structure is further improved to a small fan-like shape. The loaded fan-shaped radiating branches alter the antenna's current-flow paths for better impedance matching. The length of its branches can be calculated by the following equation, where L_s is the total length of the fan branches, and f_{s1} is the resonant frequency.

$$L_{\mathrm{S}} = W_1 + L_6 \tag{4}$$

$$f_{s1} = \frac{c}{L_{\mathrm{S}}\sqrt{\varepsilon_\gamma}} \tag{5}$$

According to Fig. 3(a), with the improvement of the antenna structure, the effective frequency band is gradually broadened, and the last bandwidth is broadened to 2–11.08 GHz. The return loss is also significantly higher. According to Fig. 3(b), finally, the isolation between each two antenna units in the operative band is basically reduced to below -15 dB.

2.2.2. Antenna Parameter Analysis

During the antenna's design phase, High Frequency Structure Simulator (HFSS) simulation and optimization of the antenna's

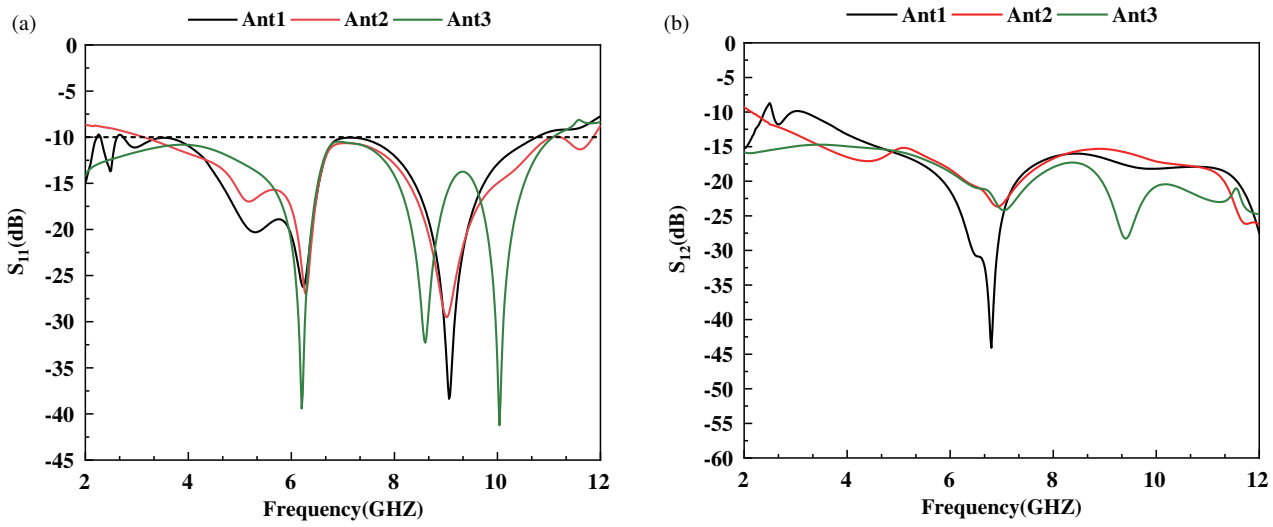

FIGURE 3. Simulation of S parameters of 3 antenna structures. (a) S_{11} and (b) S_{12}.

parameters are performed to optimize its performance. The optimization process utilizes the strategy of enhancing one parameter while keeping the values of other parameters constant. Fig. 4 displays the optimization results. From Figs. 4(a), (b), and (c), it can be observed that parameters L_1, L_6, and R primarily affect the transmission coefficients at the low-frequency band and the resonant frequencies at the high-frequency band of the antenna. Increasing L_1 initially increases the return loss at the middle and high-frequency bands, reaching the best result when L_1 is 4 mm. Gradually increasing L_6 shifts the resonant frequency of the high-frequency band to the left, with the best effect achieved when L_6 is 7 mm. Finally, increasing R shifts the resonant frequency of the high-frequency band to the left, while the return loss at the high-frequency first increases and then decreases. However, there is no significant change in the mid-frequency part as L_1, L_6, and R increase, and they all have the value of S_{11} in the low-frequency part, which first decreases and then increases. This suggests that selecting appropriate values for L_1, L_6, and R improves the antenna's impedance matching at low frequencies. In summary, the optimum values are 4 mm for L_1, 7 mm for L_6, and 2 mm for R. Ultimately, the antenna achieves a coverage frequency range of 2–11.08 GHz.

2.2.3. Antenna Surface Current Analysis

To illustrate the impact of the fan isolator, the current distributions of the three antennas are presented below at three resonant frequencies. Additionally, this analysis further examines the effects of modifications made to the radiating patch and base plate on antenna isolation. As shown in Fig. 5, under the excitation of port 1, a large amount of current is coupled to ports 2, 3, and 4 at different resonance frequencies. In addition, in Fig. 6, the change of the shape of the patch and the introduction of a circular ground plane reduce this coupling effect, and the currents on the second, third, and fourth antennas are obviously weakened, especially at the resonance frequency of 8.3 GHz, where only a fine coupling is found on the surface of the third antenna unit current, while in Fig. 7, the isolation structure of the backplane is improved to a small fan shape; the shape of the patch is further improved; almost no current is observed on the second and third antennas; and only subtle current is observed on the fourth antenna. Therefore, a high degree of isolation can be achieved with the MIMO antenna by modifying the ground plane's shape. It is clear that the fan-shaped ground plane effectively absorbs the inter-port coupling current, thereby improving the port isolation between the two monopole antennas.

3. EXPERIMENTAL SIMULATION AND MEASUREMENT

3.1. S-Parameters

Agilent N5235A vector network analyzer is utilized to determine S-parameters of the antenna. One port of the antenna is connected to a vector network tester, and the rest of the ports are connected to a 50-ohm matched load. The S-parameter measurement environment and the fabricated prototype can be seen from Fig. 8. Since each antenna cell is identical, and the antenna cells are placed two by two orthogonally to each other, thus the S-parameters are the same between antenna cells in neighboring positions and between antenna cells in diagonal positions, and the antennas are analyzed through S_{11}, S_{12}, S_{23}, and S_{13}. Based on the S-parameter curves in Fig. 9(a), the S_{11} measurement results of the antenna do not significantly deviate from the simulated results and cover the required bandwidths of 2–11.08 GHz. Regarding the reasons for the disparity between the simulated and measured results, SMA connector and transmission line losses or the test environment may cause errors resulting in small shifts in the measured frequency. The antenna isolation is further analyzed. With reference to the S_{12}-parameter curves shown in Fig. 9(b), the antenna's isolation degree is greater than 15 dB, indicating that the MIMO antenna achieves higher isolation among ports.

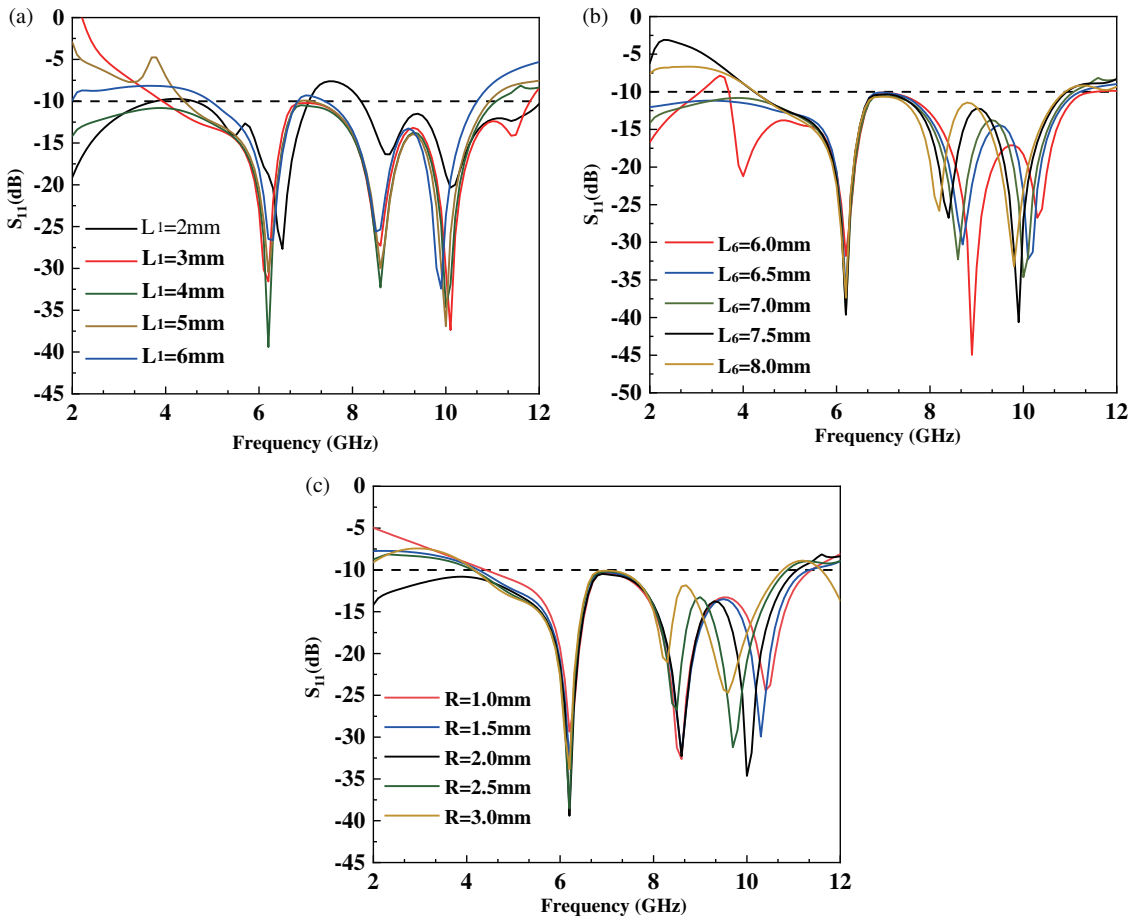

FIGURE 4. The effect of adjusted parameters on S_{11} parameters. (a) L_1, (b) L_6, and (c) R.

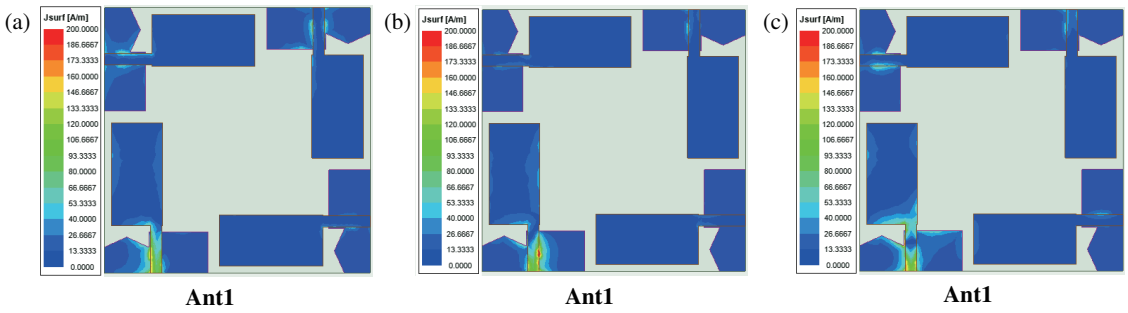

FIGURE 5. Comparison of surface current distribution of the first antenna at different resonant frequencies. (a) 6.1 GHz, (b) 8.3 GHz, (c) and 10 GHz.

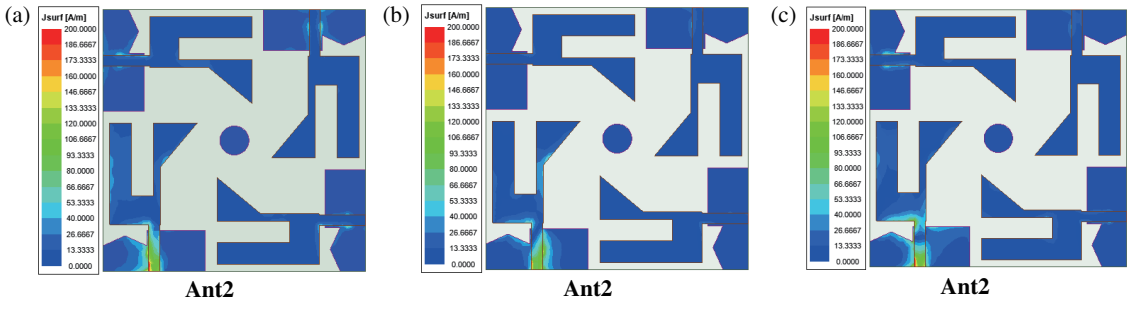

FIGURE 6. Comparison of surface current distribution of the second antenna at different resonant frequencies. (a) 6.1 GHz, (b) 8.3 GHz, (c) and 10 GHz.

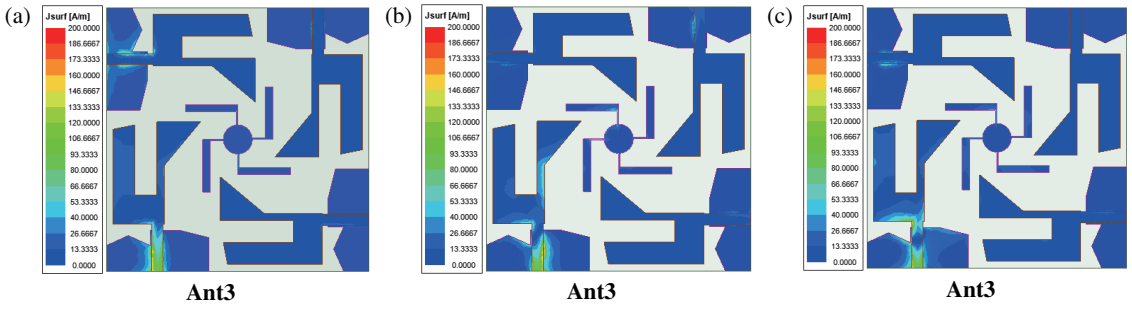

FIGURE 7. Comparison of surface current distribution of the third antenna at different resonant frequencies. (a) 6.1 GHz, (b) 8.3 GHz, (c) and 10 GHz.

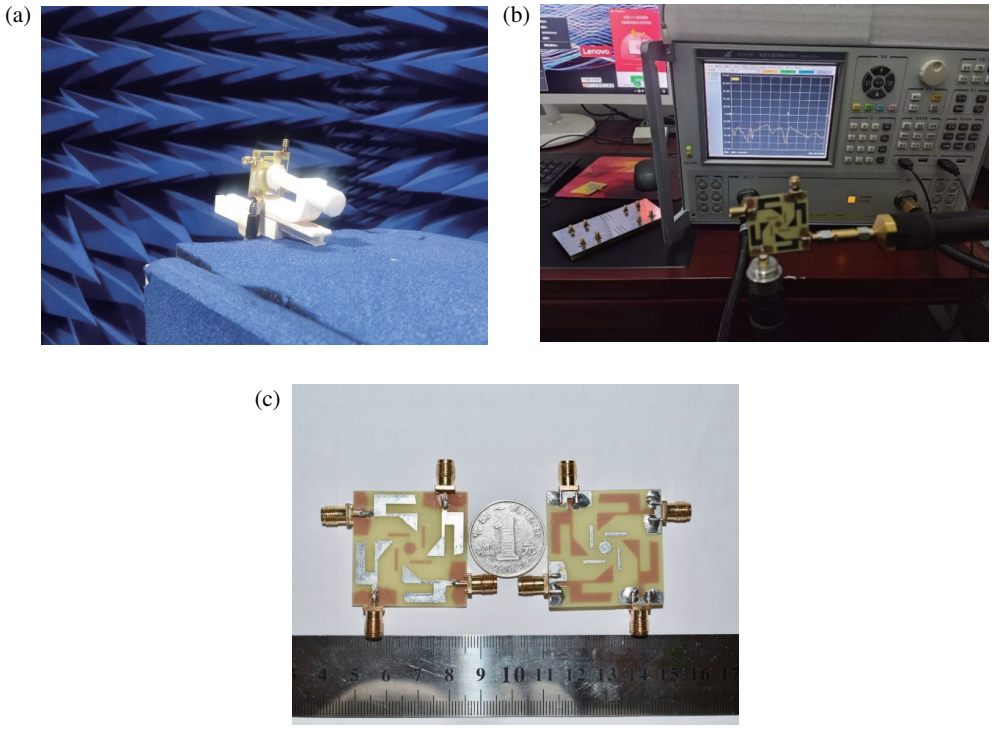

FIGURE 8. The proposed antenna (a) (b) S-parameters measurement environment and (c) Fabricated prototype.

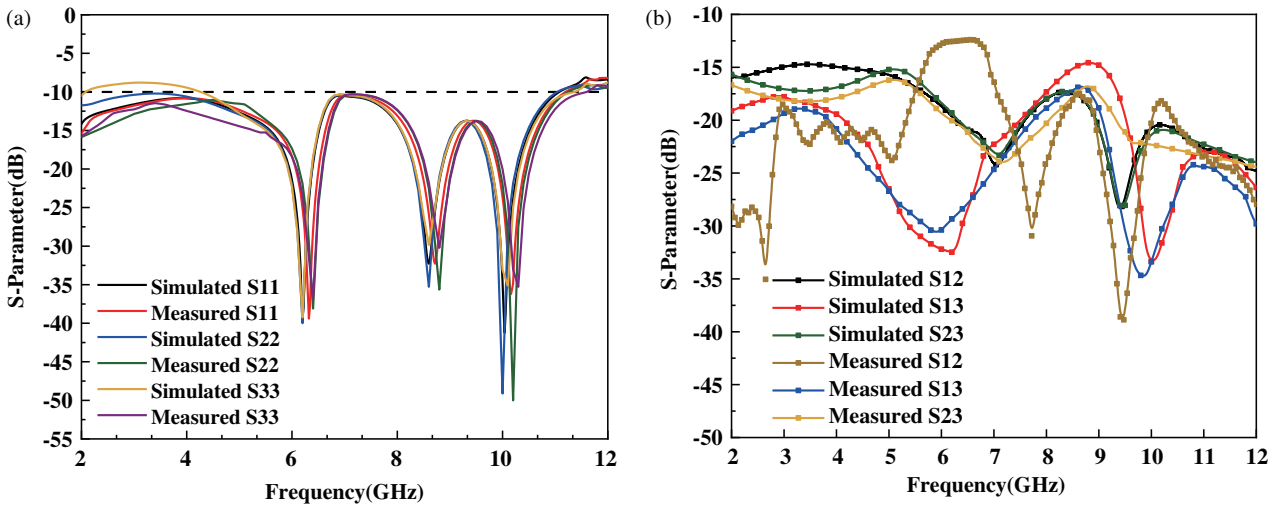

FIGURE 9. Simulated and measured S parameters of the MIMO antenna: (a) S_{11} and (b) S_{12}.

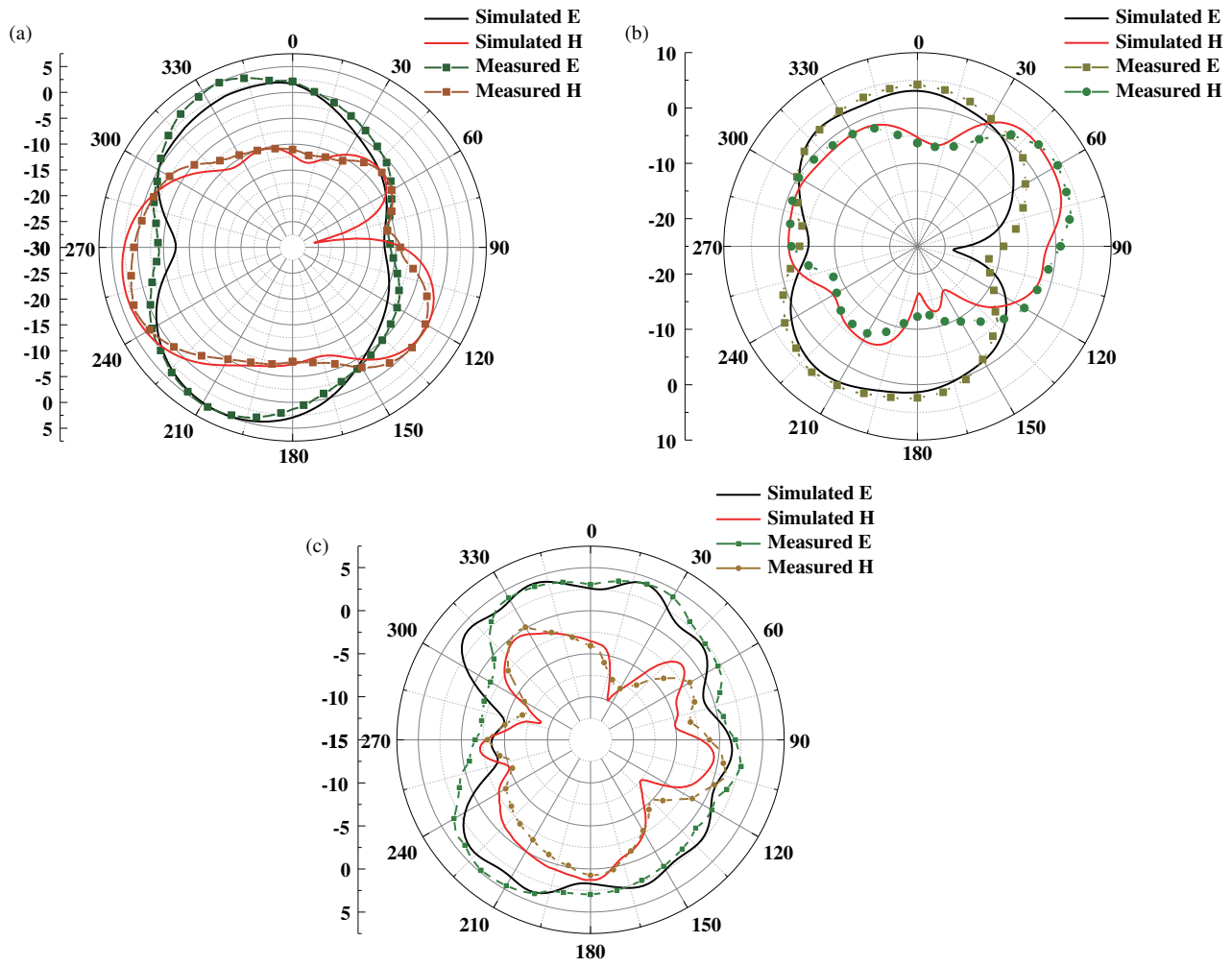

FIGURE 10. The simulated and measured radiation patterns at (a) 6.1 GHz, (b) 8.3 GHz, and (c) 10.0 GHz.

3.2. Radiation Properties

The two-dimensional radiation patterns of port 1 for the E and H planes at 6.1 GHz, 8.3 GHz, and 10 GHz are measured and presented in Fig. 10. At the resonant frequency of 6.1 GHz, the radiation pattern in the E-plane features an "8"-shaped characteristic, while in the H-plane, it takes the shape of a heart. The H-plane's maximum radiation direction is observed between 90–150 degrees and 200–330 degrees, while that of the E-plane is nearly omnidirectional, indicating commendable radiation characteristics. At 8.3 GHz, both the E-plane and H-plane present "eight"-shaped radiation characteristics, with the E-plane's maximum radiation direction extending from 0 to 40 degrees and 15 to 360 degrees. At 10 GHz, the E-plane exhibits elliptical form and nearly achieves omnidirectional radiation properties. However, the H-plane's direction is altered and resembles a flower, with the radiation gain being more prominent at 100, 180, and 330 degrees, demonstrating strong directional radiation performance. Overall, the antenna demonstrates robust radiation performance and high gain at the resonant frequencies, thus delivering excellent radiation characteristics.

The antenna's radiation efficiency and peak gain in the operational band are displayed in Fig. 11. The antenna's peak realized gain is between -2 and -6 dBi. Additionally, in the 2.5–12 GHz and 5.3–12 GHz bands, the antenna achieves a high radiation efficiency of over 70% and over 90%, respectively.

3.3. MIMO Diversity Performance

3.3.1. ECC

We estimate the effectiveness of antenna diversity using the envelope correlation coefficient (ECC), which measures the channel isolation in a wireless communication link. MIMO antenna elements are required by regulations to meet the ECC < 0.5 criteria [34], and ECC can be computed from the S-parameter with the following equation:

$$\mathrm{ECC}_{ij} = \frac{\left|S_{ii}^{*}S_{ij} + S_{ji}^{*}S_{jj}\right|^{2}}{\left(1-\left|S_{ii}\right|^{2}-\left|S_{ji}\right|^{2}\right)\left(1-\left|S_{jj}\right|^{2}-\left|S_{ij}\right|^{2}\right)} \tag{6}$$

where ECC_{ij} is the ECC between the i and j antenna elements. The ECC value of the proposed UWB-MIMO antenna is shown

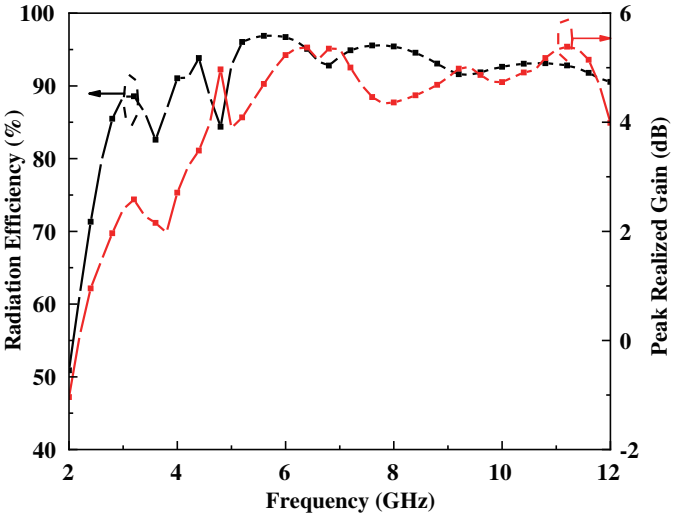

FIGURE 11. Radiation efficiency and peak realized gain of the proposed antenna.

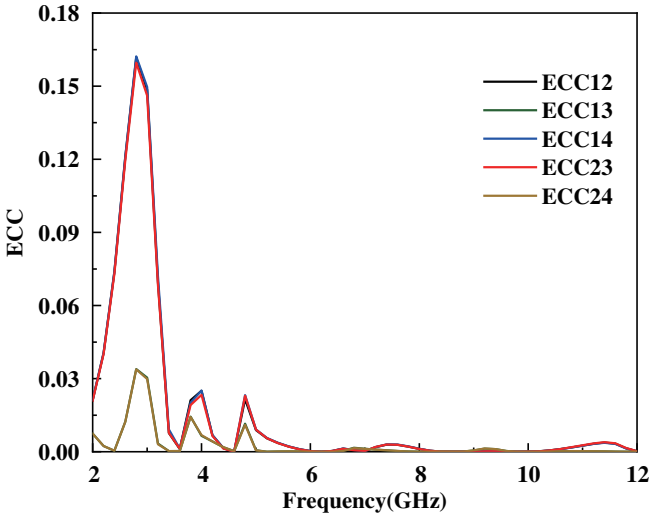

FIGURE 12. Envelope correlation coefficient of the antenna.

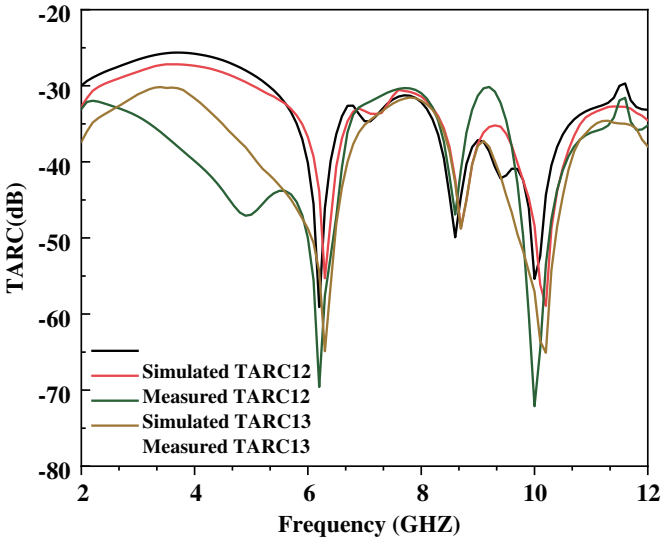

FIGURE 13. The TARC of the MIMO antenna.

in Fig. 12. ECC_{12}, ECC_{23}, and ECC_{14} are almost coincident, and ECC_{13} and ECC_{24} are almost coincident. In the frequency band, the ECC between two neighboring antenna units is less than 0.17, and the ECC between two antenna units placed diagonally is less than 0.05, which satisfies the communication requirements.

3.3.2. TARC

The efficiency of the MIMO system is evaluated using a novel metric called the Total Active Reflection Coefficient (TARC). In a multi-port antenna system, S-parameters alone are insufficient to predict the actual behavior of the system, as neighboring antenna units influence each other as well as the overall operating bandwidth and efficiency throughout operation. TARC metric, which indicates the degree to which the antenna receives all incident power, should ideally be zero. The TARC value for the MIMO system can be calculated using the following formula:

$$\mathrm{TARC}_{ij} = \sqrt{\frac{(S_{ii} + S_{ij})^2 + (S_{ji} + S_{jj})^2}{2}} \tag{7}$$

where TARC_{ij} is the TARC between the i_{th} and j_{th} antenna elements. Fig. 13 displays the TARC of the antenna. The value is lower than -20 dB in the UWB range and lower than -30 dB in the 5–12 GHz band, indicating a poor coupling effect of MIMO. The lower TARC guarantees the independence of the different channels of the MIMO system's transmitter and receiver, thereby efficiently utilizing the multipath effect to enhance the system's capacity.

3.4. Comparative Study

A detailed comparison of the size, isolation, gain, operating frequency, and ECC of the proposed UWB-MIMO antenna

TABLE 2. Performance comparison of the proposed MIMO antenna with other works.

Ref.	Size (mm × mm)	Bandwith (GHz)	Isolation (dB)	Gain (dBi)	ECC
This work	36 × 36	2–11.08	> 15	3.5–6.5	< 0.13
[5]	55×55	3.1–11.8	> 20	5.6	< 0.05
[6]	79.8 × 79.8	3.38–10.56	> 20	0–5.1	< 0.36
[7]	70 × 70	3.2–11.2	> 20	3–7.3	< 0.004
[9]	45 × 45	4.6–16.4	> 20	4–8	< 0.002
[10]	62.2 × 24.4	3.5–10.5	> 18	0–5	< 0.008
[19]	39 × 39	2.3–13.75	> 22	1.4–4.6	< 0.02
[20]	50 × 30	2.3–14.5	> 20	0–4.3	< 0.04
[22]	22 × 36	3.1–10.6	> 15	1–5	< 0.1
[30]	23 × 29	3–12	> 15	1.2–5.9	< 0.15
[31]	26 × 40	3.1–10.6	> 15	0–7	< 0.2
[35]	40 × 40	3–13.5	> 15	3.5	< 0.4
[36]	100 × 55	3.4–3.6	> 10	-	< 0.2
[37]	39 × 39	2.54–10.74	> 15	-	< 0.4

with several previously published antennas is shown in Table 2. In comparison to previous research, the suggested antenna offers a wider frequency range that is available [6, 7, 10, 22, 31]. Moreover, the size of the present work is also smaller than [5–7, 9, 10, 19], and the gain is better than [6, 30, 31]. Compared to [35–37], it has better performance in almost all aspects. Furthermore, in contrast to [5, 19, 20], the suggested antenna's decoupled construction is unique. Naturally, the proposed MIMO system also has good radiation efficiency and diversity characteristics. In conclusion, with comparable antenna performance, the antenna has better performance and is very suitable for indoor communication. The comparison of performances between the suggested UWB-MIMO antenna and previous work is displayed in Table 2.

4. CONCLUSION

In this paper, a UWB MIMO antenna with high isolation is designed for the use in a variety of wireless communication bands. Using a U-shaped radiating patch and a rectangular backplane structure with cut-outs and a fan-shaped isolation structure, the antenna is able to achieve band characteristics covering the range 2–11.08 GHz. Antenna units are placed orthogonal to each other to obtain a more compact structure and excellent isolation, and the backplane is loaded with a fan-shaped metal structure to absorb ground current, further enhancing the isolation between the antennas, and ultimately achieving an overall isolation of better than 15 dB. Finally, the four-port UWB multiple-input, multiple-output antenna is characterized by its compact structure, small size, high radiation efficiency, and acceptable ECC. From the above results, the proposed antenna is suitable for a wide range of communication applications, including cellular mobile communication, satellite communication, wireless local area networks, and others.

ACKNOWLEDGEMENT

This work was supported in part by the Anhui Provincial Natural Science Foundation under Grant No. 2108085MF200, in part by the Natural Science Research Project of Anhui Educational Committee under No. 2022AH051583 and No. 2022AH052138.

REFERENCES

[1] Yuan, X.-T., Z. Chen, T. Gu, and T. Yuan, "A wideband PIFA-pair-based MIMO antenna for 5G smartphones," *IEEE Antennas and Wireless Propagation Letters*, Vol. 20, No. 3, 371–375, 2021.

[2] Docket, E. T., "Revision of part 15 of the commissions rules regarding ultra-wideband transmission systems," Docket 98–153, Federal Communications Commission, Tech. Rep., 2002.

[3] Kaiser, T., F. Zheng, and E. Dimitrov, "An overview of ultra-wide-band systems with MIMO," *Proceedings of the IEEE*, Vol. 97, No. 2, 285–312, 2009.

[4] Kareemulla, S. and V. Kumar, "Diversity performance of band notched ultra-wideband MIMO antenna," *Optik*, Vol. 272, 170128, 2023.

[5] Abbas, A., M. A. Sufian, J. Jung, A. Uktam, J. Lee, and N. Kim, "A triple band notched UWB MIMO antenna with improved performance," in *2022 Asia-Pacific Microwave Conference (APMC)*, 482–484, 2022.

[6] Jayant, S. and G. Srivastava, "Close-Packed quad-element triple-band-notched UWB MIMO antenna with upgrading capability," *IEEE Transactions on Antennas and Propagation*, Vol. 71, No. 1, 353–360, 2023.

[7] Yao, Y., Y. Shao, J. Zhang, and J. Zhang, "A transparent antenna using metal mesh for UWB MIMO applications," *IEEE Transactions on Antennas and Propagation*, Vol. 71, No. 5, 3836–3844, 2023.

[8] Desai, A., J. Kulkarni, M. M. Kamruzzaman, S. Hubálovský, H.-T. Hsu, and A. A. Ibrahim, "Interconnected CPW fed flexible 4-port MIMO antenna for UWB, X, and Ku band applications," *IEEE Access*, Vol. 10, 57 641–57 654, 2022.

[9] Kumar, P., S. Pathan, S. Vincent, O. P. Kumar, N. Yashwanth, P. Kumar, P. R. Shetty, and T. Ali, "A compact quad-port UWB MIMO antenna with improved isolation using a novel mesh-like decoupling structure and unique DGS," *IEEE Transactions on Circuits and Systems II: Express Briefs*, Vol. 70, No. 3, 949–953, 2023.

[10] Jayant, S., G. Srivastava, and M. Khari, "8-Port MIMO antenna having two notched bands for chipless UWB-RFID tags," *IEEE Journal of Radio Frequency Identification*, Vol. 6, 355–360, 2022.

[11] Jayant, S., G. Srivastava, and S. Kumar, "Quad-port UWB MIMO footwear antenna for wearable applications," *IEEE Transactions on Antennas and Propagation*, Vol. 70, No. 9, 7905–7913, 2022.

[12] Zhang, K., Z. H. Jiang, W. L. Zhou, P. Peng, and W. Hong, "A compact, band-notched ultra-wideband fully-recessed antenna with pattern diversity for V2X communications," *IEEE Open Journal of Antennas and Propagation*, Vol. 3, 1302–1312, 2022.

[13] Paul, P. M., K. Kandasamy, M. S. Sharawi, and B. Majumder, "Dispersion-engineered transmission line loaded slot antenna for UWB applications," *IEEE Antennas and Wireless Propagation Letters*, Vol. 18, No. 2, 323–327, 2019.

[14] Zhu, L., R. Fu, and K.-L. Wu, "A novel broadband microstrip-fed wide slot antenna with double rejection zeros," *IEEE Antennas and Wireless Propagation Letters*, Vol. 2, 194–196, 2003.

[15] Lui, W. J., C. H. Cheng, Y. Cheng, and H. B. Zhu, "A novel broadband multislot antenna fed by microstrip line," *Microwave and Optical Technology Letters*, Vol. 45, No. 1, 55–57, 2005.

[16] Zhang, J.-Y., F. Zhang, W.-P. Tian, and Y.-L. Luo, "ACS-fed UWB-MIMO antenna with shared radiator," *Electronics Letters*, Vol. 51, No. 17, 1301–1302, 2015.

[17] Huang, X. D., C. H. Cheng, and L. Zhu, "An ultrawideband (UWB) slotline antenna under multiple-mode resonance," *IEEE Transactions on Antennas and Propagation*, Vol. 60, No. 1, 385–389, 2012.

[18] Chandel, R., A. K. Gautam, and K. Rambabu, "Tapered fed compact UWB MIMO-diversity antenna with dual band-notched characteristics," *IEEE Transactions on Antennas and Propagation*, Vol. 66, No. 4, 1677–1684, 2018.

[19] Tang, Z., X. Wu, J. Zhan, S. Hu, Z. Xi, and Y. Liu, "Compact UWB-MIMO antenna with high isolation and triple band-notched characteristics," *IEEE Access*, Vol. 7, 19 856–19 865, 2019.

[20] Iqbal, A., O. A. Saraereh, A. W. Ahmad, and S. Bashir, "Mutual coupling reduction using F-shaped stubs in UWB-MIMO antenna," *IEEE Access*, Vol. 6, 2755–2759, 2017.

[21] Wang, L., Z. Du, H. Yang, R. Ma, Y. Zhao, X. Cui, and X. Xi, "Compact UWB MIMO antenna with high isolation using fence-type decoupling structure," *IEEE Antennas and Wireless Propagation Letters*, Vol. 18, No. 8, 1641–1645, 2019.

[22] Lu, Z., H. Lin, Z. Wang, W. Nie, and W. Mu, "Compact ACS-fed MIMO antenna with dual-band notch characteristics for UWB applications," *International Journal of Microwave and Wireless Technologies*, 1–9, 2023.

[23] Durukan, T. and Y. Altuncu, "A compact 4 × 4 reconfigurable MIMO antenna design with adjustable suppression of certain frequency bands within the UWB frequency range," *AEU — International Journal of Electronics and Communications*, Vol. 170, 154848, 2023.

[24] Huang, J., G. Dong, Q. Cai, Z. Chen, L. Li, and G. Liu, "Dual-band MIMO antenna for 5G/WLAN mobile terminals," *Micromachines*, Vol. 12, No. 5, 489, 2021.

[25] Mao, C.-X. and Q.-X. Chu, "Compact coradiator UWB-MIMO antenna with dual polarization," *IEEE Transactions on Antennas and Propagation*, Vol. 62, No. 9, 4474–4480, 2014.

[26] Radhi, A. H., R. Nilavalan, Y. Wang, H. S. Al-Raweshidy, A. A. Eltokhy, and N. A. Aziz, "Mutual coupling reduction with a wideband planar decoupling structure for UWB–MIMO antennas," *International Journal of Microwave and Wireless Technologies*, Vol. 10, No. 10, 1143–1154, 2018.

[27] Jaglan, N., S. D. Gupta, E. Thakur, D. Kumar, B. K. Kanaujia, and S. Srivastava, "Triple band notched mushroom and uniplanar EBG structures based UWB MIMO/Diversity antenna with enhanced wide band isolation," *AEU — International Journal of Electronics and Communications*, Vol. 90, 36–44, 2018.

[28] Chithradevi, R. and B. S. Sreeja, "A compat UWB MIMO antenna with high isolation and low correlation for wireless applications," in *2017 IEEE International Conference on Antenna Innovations & Modern Technologies for Ground, Aircraft and Satellite Applications (iAIM)*, 1–4, 2017.

[29] Nikam, B. V. and M. R. Jadhav, "A compact quad port band-notched MIMO antenna for Wi-Max applications with low mutual coupling," *Progress In Electromagnetics Research C*, Vol. 104, 53–67, 2020.

[30] Mathur, R. and S. Dwari, "4-port extended ultrawideband MIMO/diversity antenna for indoor and outdoor wireless communication," in *2023 IEEE Wireless Antenna and Microwave Symposium (WAMS)*, 1–5, 2023.

[31] Suresh, A. C. and T. S. Reddy, "A flower shaped miniaturized 4 x 4 MIMO antenna for UWB applications using characteristic mode analysis," *Progress In Electromagnetics Research C*, Vol. 119, 219–233, 2022.

[32] Luo, S., D. Wang, Y. Chen, E. Li, and C. Jiang, "A compact dual-port UWB-MIMO antenna with quadruple band-notched characteristics," *AEU — International Journal of Electronics and Communications*, Vol. 136, 153770, 2021.

[33] Sharma, N. and S. S. Bhatia, "Metamaterial inspired fidget spinner-shaped antenna based on parasitic split ring resonator for multi-standard wireless applications," *Journal of Electromagnetic Waves and Applications*, Vol. 34, No. 10, 1471–1490, 2020.

[34] Singh, P. P. and S. K. Sharma, "Design and fabrication of a triple band microstrip antenna for WLAN, satellite TV and radar applications," *Progress In Electromagnetics Research C*, Vol. 117, 277–289, 2021.

[35] Khan, A. A., S. A. Naqvi, M. S. Khan, and B. Ijaz, "Quad port miniaturized MIMO antenna for UWB 11 GHz and 13 GHz frequency bands," *AEU — International Journal of Electronics and Communications*, Vol. 131, 153618, 2021.

[36] Ullah, R., S. Ullah, B. Kamal, and R. Ullah, "A four-port multiple input multiple output (MIMO) antenna for future 5G smartphone applications," in *2019 International Conference on Electrical, Communication, and Computer Engineering (ICECCE)*, 1–5, 2019.

[37] Kaur, H., H. S. Singh, and R. Upadhyay, "Design and analysis of planar four-port UWB-MIMO antenna with band-rejection capability," *International Journal of Microwave and Wireless Technologies*, 1–13, 2023.